JOURNAL OF MATERIALS SCIENCE 27 (1992) 5453–5462

Failure behaviour of particulate-reinforced aluminium alloy composites under uniaxial tension

J. C. LEE, K. N. SUBRAMANIAN
Department of Metallurgy, Mechanics and Materials Science, Michigan State University, East Lansing, MI 48824, USA

Tensile tests were carried out at room temperature on 6061–aluminium alloy reinforced with SiC and Al_2O_3 particulates. Although a significant increase in strength could be achieved by introducing ceramic reinforcements into the aluminium alloy matrix, it is associated with a substantial decrease in fracture strain. In order to understand the reason for the inferior ductility of such composites, analytical solutions were obtained using a simple composite model. SEM studies were carried out on the side surfaces of the fractured specimens to verify the proposed failure behaviour. Failure modes observed to operate in such composites under uniaxial tension are described.

1. Introduction

The addition of moderate amounts of SiC particulate (SiC_p) and Al_2O_3 particulate ($(Al_2O_3)_p$), usually less than 30 vol %, into molten aluminium alloy has been found to result in significant increases in the strength and elastic modulus [1–7], fatigue resistance [8–10], and wear resistance [11], as well as improved high-temperature properties [12–14] of the composites. However, it also results in substantial decrease in the ductility and, consequently, the fracture toughness of the composites. This has been the main drawback for the wide use of such metal matrix composites reinforced with ceramic reinforcements. Several studies have been carried out to improve the ductility and the fracture toughness of ceramic-reinforced metal matrix composites by modified processing techniques [3, 8, 15–20]. Large differences in the properties between the reinforced and the unreinforced aluminium alloys still exist due to large differences in the properties of the matrix and the reinforcements. Poor ductility and fracture toughness of such metal matrix composites are attributed to the operative failure mechanisms.

Nutt and Duva [21], in their *in situ* TEM studies on SiC whisker-reinforced aluminium matrix composites (SiC_w/Al composites), observed that the void nucleated at the corner of the whisker ends and grew towards the centres of the whisker ends. However, the void formation along the long sides of the SiC_w/Al interface, which are parallel to the tensile direction, was not observed. Based on the above experimental results, void nucleation at the SiC_w/Al interface (i.e. interfacial debonding) was proposed as the important failure mechanism in the SiC_w/Al composites [21–23].

You *et al.* [24] proposed another failure mechanism of the SiC_p/Al composite on the basis of the observations on the tensile fracture surfaces. In their study, the number of cracked SiC_p and debonded interfaces were counted at the fracture surface. From this analysis, the number of cracked SiC_p was found to be more than twice the number of the debonded interfaces. Extensive plastic deformation in the matrix between SiC_p was also observed from the side surfaces of the tensile specimen, at regions adjacent to the fracture surface. Based on the above observations, they proposed the matrix failure of the composite due to nucleation, growth and coalescence of voids as a dominant failure mechanism of the SiC_p/Al composites. As a consequence, the cracking of SiC_p and debonding of SiC_p/Al interface were attributed to the matrix failure.

Based on the examination of fractographs of pulled-out SiC_w that are coated with the matrix material, Christman *et al.* [9, 25] have proposed ductile failure in the matrix near the SiC_w as one of the operating failure mechanisms of such composites.

Janowski and Pletaka [26] had studied interfacial microstructures of aluminium alloy composites reinforced with SiC_p and $(Al_2O_3)_p$ and their effect on the tensile properties of such composites. Failure modes present in particulate-reinforced composites were observed to change depending on the characteristics of the interfacial microstructures. Amorphous reaction layers formed at the $(Al_2O_3)_p$/Al interface were found to degrade interfacial bonding, and thereby result in inferior strength and ductility of such composities.

The purpose of the present investigation was to study the general failure behaviour of particulate-reinforced metal matrix composites under uniaxial tension.

2. Experimental procedure

The materials used in this study, 6061 aluminium alloys reinforced with 10 vol % SiC_p and $(Al_2O_3)_p$,

0022–2461

were obtained as extruded cylindrical bars. Sheet tensile specimens were machined with the tensile direction oriented both parallel (longitudinal) and perpendicular (transverse) to the extrusion direction, and polished with abrasive papers and rotating laps. They were then T6 heat treated according to the conditions listed in Table I. The oxidation layer formed during heat treatment was removed by polishing with diamond abrasives.

Tensile tests were carried out with an Instron operated at a constant crosshead speed of 0.1 cm min^{-1} in air at room temperature. The fracture surface and the side surfaces of tensile specimens were examined by optical and scanning electron microscopic techniques.

3. Results

Some of tensile properties of the reinforced and the unreinforced aluminium alloy are presented in Table II.

Although considerable increase in the elastic modulus and strength result due to reinforcements, they are accompanied by substantial decrease in the fracture strain. In order to understand the reasons for the inferior ductility of the composite, studies were carried out to characterize the interfacial debonding and particulate cracking. A significant number of debonded interfaces could be observed from the subsurface of the fractured specimens, as shown in Fig. 1, for which deep etching was carried out. Such interfacial debondings were formed in a direction perpendicular to the tensile loading as shown in Fig. 1b and c.

Finely polished tensile specimens were prepared and tested with an Instron to observe the particulate cracking and possible matrix failure at the composite surface. Observations made on the side surfaces of the fractured tensile specimens, especially in regions adjacent to fracture, revealed significant amounts of microcracks at SiC_p, as shown in Fig. 2. Microcracks initiated from the matrix were not observed in the present study. Most of the cracks were formed at SiC_p and $(Al_2O_3)_p$ in the form of interfacial debonding and particulate cracking, or sometimes in the form of ductile failure near the reinforcement. Although severe plastic deformation can be observed in the matrix near the region of cracked SiC_p, particulate cracking was always found to precede the matrix failure. The micrographs exhibiting the initiation of cracks in SiC_p and $(Al_2O_3)_p$ in the tensile specimens are shown in Fig. 3a and b.

TABLE I T6 heat-treatment condition used in the present study

	SiC_p/Al composite	$(Al_2O_3)_p$/Al composite
Solution treatment	530 °C, 70 min	560 °C, 60 min
RT ageing	24 °C, 48 h	24 °C, 65 h
Artificial ageing	200 °C, 10 h[a]	170 °C, 14 h[b]

[a] Overaged condition.
[b] Peak-aged condition.

TABLE II The tensile properties of T6 heat-treated reinforced and unreinforced aluminium alloy

Material	Direction[a]	E(GPa)	σ_{ys}(MPa)	σ_{uts}(MPa)	ε_f(%)
SiC_p/Al	T	–	269.5	323.0	2.8
	L	–	302.0	368.6	5.3
$(Al_2O_3)_p$/Al	T	80.6[b]	285.0	345.2	2.5
	L	79.9[b]	301.5	364.5	9.0
6061 Al		68.0[b]	265.5	310.5	20.0

[a] T, transverse direction; L, Longitudinal direction.
[b] Values measured by sonic resonance method.

4. Theoretical background

Most three-dimensional engineering problems can be analysed using a two-dimensional approach, because most failures are initiated at free surfaces, where the largest stresses develop. Consider a large thin plate having a circular inclusion, whose elastic constants and thermal expansion coefficient are different from those of the matrix. Uniform uniaxial loading is applied at infinity on the composite system as shown in Fig. 4a. One can solve this problem by superposing the stress function due to uniaxial loading and stress function due to the inelastic strain caused by thermal expansion mismatch as in Fig. 4b. Although the solutions for the problems given in Sections 4.1 and 4.2 can be found elsewhere [27], detailed calculation steps with slightly different methods will be presented in order to utilize the intermediate solutions to the analysis.

4.1 Large plate having a circular inclusion with different elastic constants subjected to uniaxial tension

Consider a plate having a small circular elastic inclusion of radius a, which is subjected to uniaxial tension. Under such conditions, the boundary conditions at infinity ($r = \infty$) are given by

$$\sigma_{rr}(\infty, \theta) = \sigma_0(1 + \cos 2\theta)/2 \quad (1a)$$

$$\sigma_{r\theta}(\infty, \theta) = -\sigma_0 \sin 2\theta/2 \quad (1b)$$

$$\sigma_{\theta\theta}(\infty, \theta) = \sigma_0(1 - \cos 2\theta)/2 \quad (1c)$$

The Airy stress function, Φ, for this case can be given as a linear combination of function of polar coordinates r and θ. Matrix part of this function, Φ^{m^1}, is

$$\Phi^{m^1}(r, \theta) = \frac{\sigma_0}{4} r^2(1 - \cos 2\theta) + \frac{\sigma_0}{4}\left[Aa^2 \log r + Ba^2 \cos 2\theta + Ca^4\left(\frac{\cos 2\theta}{r^2}\right)\right] \quad (2)$$

where A, B, and C are constants, and superscript m^1 denotes matrix under applied uniaxial loading. One can notice that the first term in Equation 2 describes the undisturbed field (when there is no inclusion in the matrix), and the last three terms describe the local disturbance due to the discontinuity (i.e. inclusion) in the elastic medium. However, according to Saint

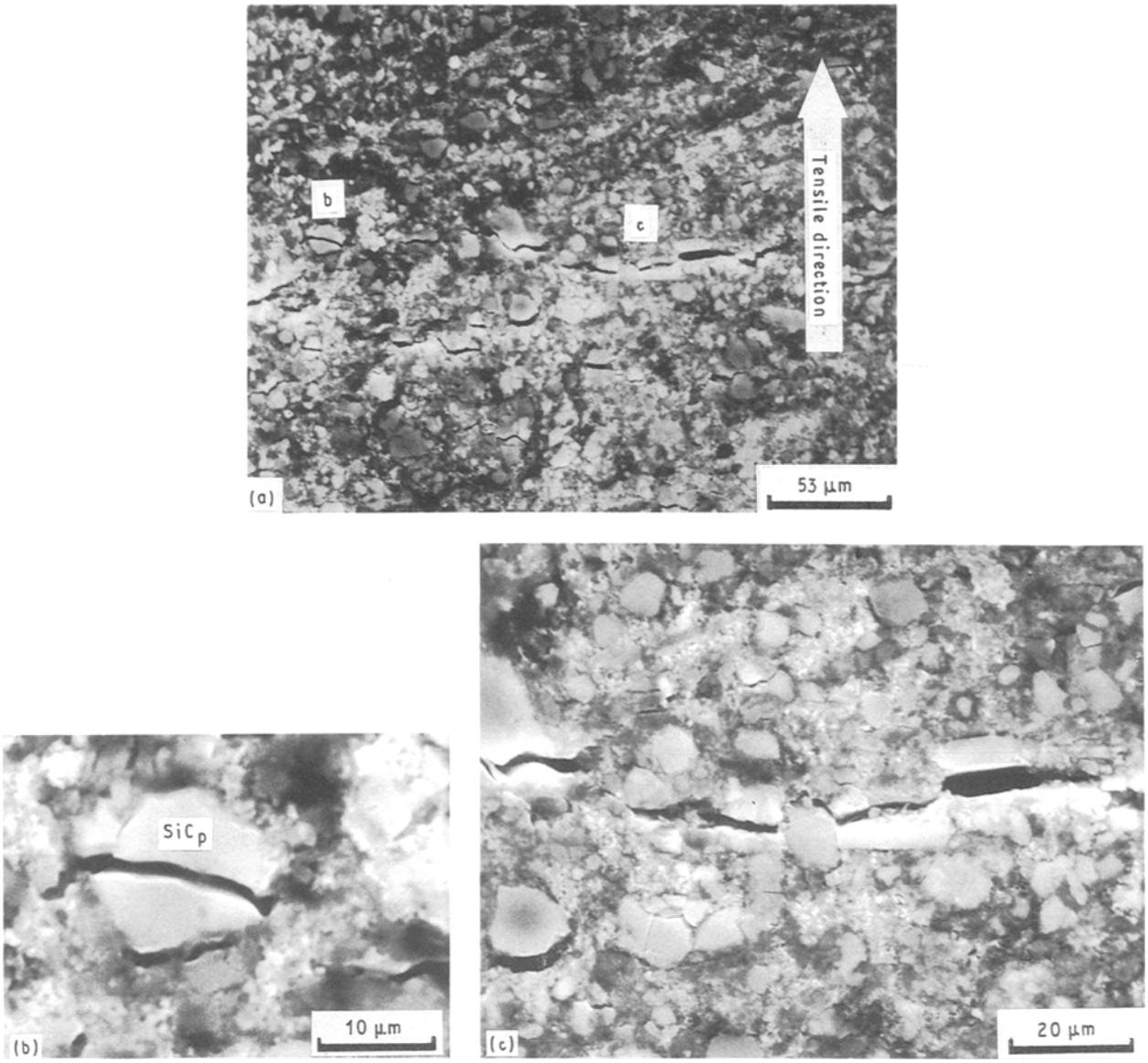

Figure 1 (a) Scanning electron micrograph showing crack development in a tensile specimen of SiC_p/Al composite (etched with HCl to reveal the subsurface region). (b) Interfacial debonding and particulate cracking. Note the crack propagation into the matrix in front of the particulate crack. (c) Joining of particulate crack and debonded interface.

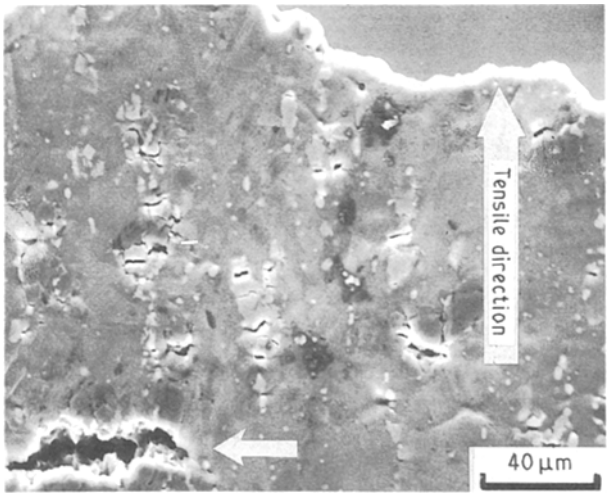

Figure 2 Scanning electron micrograph of the fractured SiC_p/Al composite showing void formation due to joining of opened cracks, indicated by an arrow. Note that cracks are formed perpendicular to the tensile direction and the number of particulate cracks is significantly more than the debonded interfaces.

Venant's principle, the disturbance caused by discontinuity will be negligible at distances which are larger compared to the radius of the discontinuity.

The Airy stress function for the inclusion can be given as

$$\Phi^{i^1}(r, \theta) = \frac{\sigma_0}{4}\left(Dr^2 + Er^2 \cos 2\theta + \frac{F}{a^2} r^4 \cos 2\theta \right) \quad (3)$$

where D, E and F are constants, and the superscript i^1 denotes inclusion under applied uniaxial loading. The stress components, σ_{ij}, can be obtained directly from the given Airy stress functions, and the corresponding strain, e_{ij}, and displacement components, u_i, can be determined from the Hooke's law and strain–displacement relationships, respectively. Thus, the resultant stresses and displacements in the matrix and the inclusion are

$$\sigma_{rr}^{m^1} = (\sigma_0/2)[1 + Aa^2/r^2 + (1 - 2Ba^2/r^2 - 3Ca^4/r^4)\cos 2\theta] \quad (4a)$$

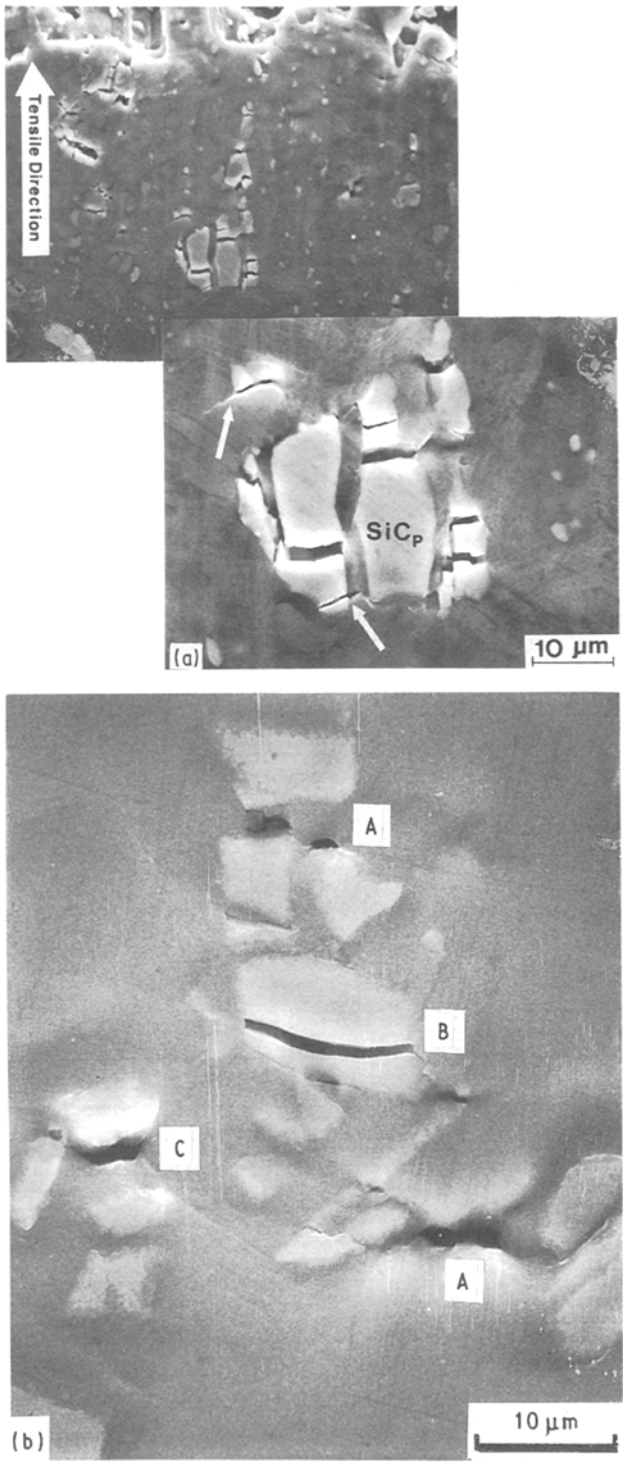

Figure 3 (a) Particulate cracks in SiC_p/Al composite which are opened up due to tensile loading. Arrows indicate the initiation of the crack propagation into the matrix. (b) Particulate cracks and interfacial debonding in $(Al_2O_3)_p$/Al composite caused by tensile loading. A, interfacial debonding; B, particulate cracking; C, matrix adhering to $(Al_2O_3)_p$.

$$\sigma_{r\theta}^{m^1} = (-\sigma_0/2)[1 + Ba^2/r^2 + 3Ca^4/r^4]\sin 2\theta \quad (4b)$$

$$\sigma_{\theta\theta}^{m^1} = (\sigma_0/2)[1 - Aa^2/r^2 - (1 - 3Ca^4/r^4)\cos 2\theta] \quad (4c)$$

$$u_r^{m^1} = (\sigma_0/8\mu^m)\{(\kappa^m - 1)r - 2Aa^2/r + [2r + B(\kappa^m + 1)a^2/r + 2Ca^4/r^3]\cos 2\theta\} \quad (4d)$$

$$u_\theta^{m^1} = (\sigma_0/8\mu^m)[-2r - B(\kappa^m - 1)a^2/r + 2Ca^4/r^3]\sin 2\theta \quad (4e)$$

$$\sigma_{rr}^{i^1} = (\sigma_0/2)(D - E\cos 2\theta) \quad (4f)$$

$$\sigma_{r\theta}^{i^1} = (\sigma_0/2)(E + 3Fr^2/a^2)\sin 2\theta \quad (4g)$$

$$\sigma_{\theta\theta}^{i^1} = (\sigma_0/2)[D + (E + 6Fr^2/a^2)\cos 2\theta] \quad (4h)$$

$$u_r^{i^1} = (\sigma_0/8\mu^i)\{D(\kappa^i - 1)r - [2Er - F(\kappa^i - 3)r^3/a^2]\cos 2\theta\} \quad (4i)$$

$$u_r^{i^1} = (\sigma_0/8\mu^i)[2Er + F(\kappa^i + 3)r^3/a^2]\sin 2\theta \quad (4j)$$

In order to determine the constants in Equation 4, appropriate boundary conditions for the composite system should be set up at the interface, assuming perfect interfacial bonding.

Because the stresses and the displacements have to be continuous at the interface, boundary conditions at the matrix–inclusion interface ($r = a$) are

$$\sigma_{rr}^{m^1}(a, \theta) = \sigma_{rr}^{i^1}(a, \theta), \quad \sigma_{r\theta}^{m^1}(a, \theta) = \sigma_{r\theta}^{i^1}(a, \theta) \quad (5a)$$

$$u_r^{m^1}(a, \theta) = u_r^{i^1}(a, \theta), \quad u_\theta^{m^1}(a, \theta) = u_\theta^{i^1}(a, \theta) \quad (5b)$$

Solving the boundary conditions, one can obtain the constants as

$$A = [(\kappa^m - 1) - \Gamma(\kappa^i - 1)]/[\Gamma(\kappa^i - 1) + 2] \quad (6a)$$

$$B = 2(\Gamma - 1)/(\Gamma + \kappa^m) \quad (6b)$$

$$C = (1 - \Gamma)/(\Gamma + \kappa^m) \quad (6c)$$

$$D = [\kappa^m + 1]/[\Gamma(\kappa^i - 1) + 2] \quad (6d)$$

$$E = -(\kappa^m + 1)/(\Gamma + \kappa^m) \quad (6e)$$

$$F = 0 \quad (6f)$$

where $\Gamma = \mu^m/\mu^i$

4.2. Large plate having a circular inclusion with different thermal expansion coefficient

If the system involves inelastic strain caused by thermal expansion coefficient mismatch, it will produce an inelastic stress on the body. Some important results will be listed without derivation, because the exact solutions for this problem can be found elsewhere [27]. The compressive stress, $-P$, at the inclusion/matrix interface, resulting from thermal expansion mismatch, is obtained as

$$P = [4\mu^m\mu^i(1 + \eta)\Delta\alpha\Delta T]/[2\mu^i + (\kappa^i - 1)\mu^m] \quad (7)$$

Stress components for the matrix and inclusion are determined as

$$\sigma_{rr}^{m^2}(r, \theta) = -Pa^2/r^2 \quad (8a)$$

$$\sigma_{\theta\theta}^{m^2}(r, \theta) = Pa^2/r^2 \quad (8b)$$

$$\sigma_{r\theta}^{m^2}(r, \theta) = 0 \quad (8c)$$

$$\sigma_{rr}^{i^2}(r, \theta) = -P \quad (8d)$$

$$\sigma_{\theta\theta}^{i^2}(r, \theta) = -P \quad (8e)$$

$$\sigma_{r\theta}^{i^2}(r, \theta) = 0 \quad (8f)$$

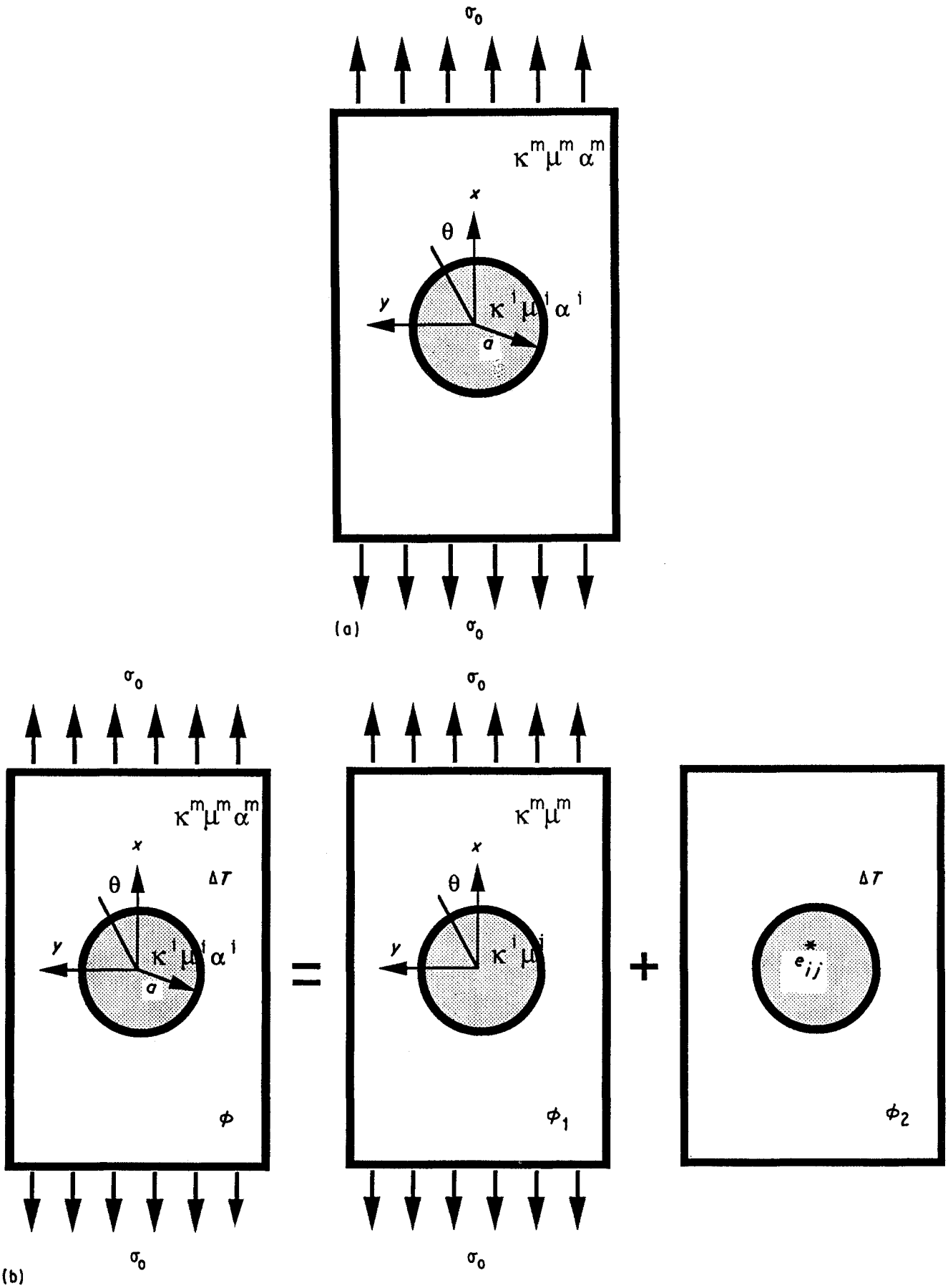

Figure 4 (a) Two-dimensional composite model; a large thin plate having a circular inclusion with different elastic constants, (κ, μ), and thermal expansion coefficients, α, subjected to uniaxial tension, σ_0, where μ is the shear modulus, α is the thermal expansion coefficient, $\kappa = (3 - 4\nu)$ for plane strain, $\kappa = (3 - \nu)/(1 + \nu)$ for plane stress. (b) Schematics drawings of the superposition of stresses caused by external loading and thermal expansion coefficient mismatch.

where superscripts m^2 and i^2 represent matrix and inclusion parts under inelastic contribution due to thermal expansion coefficient mismatch.

Hence, from the results in Sections 4.1 and 4.2, the total stress and displacement should be the sum of the elastic and the inelastic terms

$$\sigma_{ij}^{I} = \sigma_{ij}^{i^1} + \sigma_{ij}^{i^2}, \quad \sigma_{ij}^{M} = \sigma_{ij}^{m^1} + \sigma_{ij}^{m^2} \tag{9a}$$

$$u_i^{I} = u_i^{i^1} + u_i^{i^2}, \quad u_i^{M} = u_i^{m^1} + u_i^{m^2}. \tag{9b}$$

Above stress components evaluated in the polar coordinate can be transformed into the stress components in the Cartesian coordinate using the transformation laws

$$\sigma_{xx} = \sigma_{rr}\cos^2\theta - 2\sigma_{r\theta}\cos\theta\sin\theta + \sigma_{\theta\theta}\sin^2\theta \tag{10a}$$

$$\sigma_{yy} = \sigma_{rr}\sin^2\theta + 2\sigma_{r\theta}\cos\theta\sin\theta + \sigma_{\theta\theta}\cos^2\theta \tag{10b}$$

$$\sigma_{xy} = (\sigma_{rr} - \sigma_{\theta\theta})\cos\theta\sin\theta + \sigma_{r\theta}(\cos^2\theta - \sin^2\theta) \tag{10c}$$

5. Analysis and discussion

5.1. Stress concentration and load transfer

When a discontinuity is present in a body, local stress disturbances will be developed near the discontinuity. However, the extent and shape of stress disturbance near the discontinuity depend on the geometry of the discontinuity, and the difference in the elastic constants and thermal expansion coefficients between the matrix and the discontinuity. For example, when a large thin plate having a discontinuity with smaller elastic modulus than the matrix (such as a hole) is subjected to uniaxial tension, a stress concentration will occur at the matrix near the equator of the hole, and decrease rapidly at distances away from the hole. However, in the case of a large thin plate having a discontinuity with an elastic modulus higher than that of the matrix, a stress concentration occurs at the discontinuity rather than in the matrix. Such stress disturbances for an SiC inclusion in an aluminium alloy matrix are illustrated in Figs 5 and 6. The elastic constants and thermal expansion coefficients of 6061 aluminium alloy and SiC used for the calculations are given in Table III. Although, computations were carried out for SiC_p/Al composite only, trends exhibited by $(Al_2O_3)_p$/Al composite are expected to be similar. The stress acting on the matrix near the equator of the inclusion is found to be lower than the applied tensile stress due to the load transfer to the inclusion through the interface. However, the stress

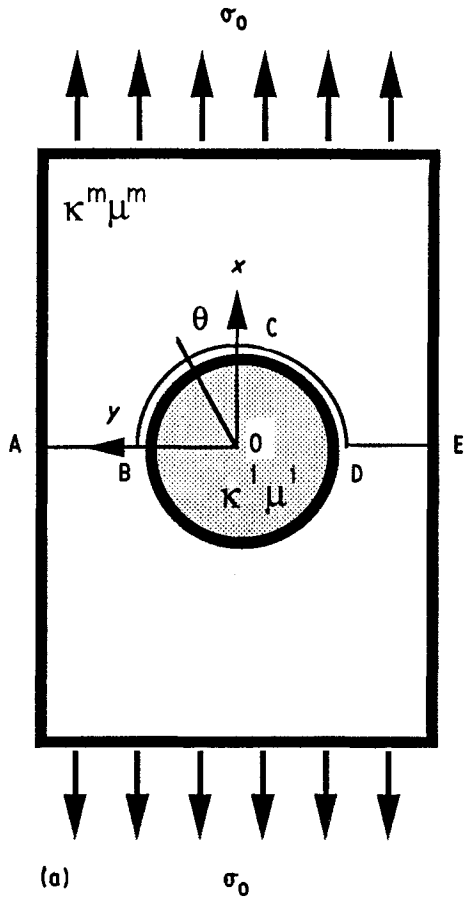

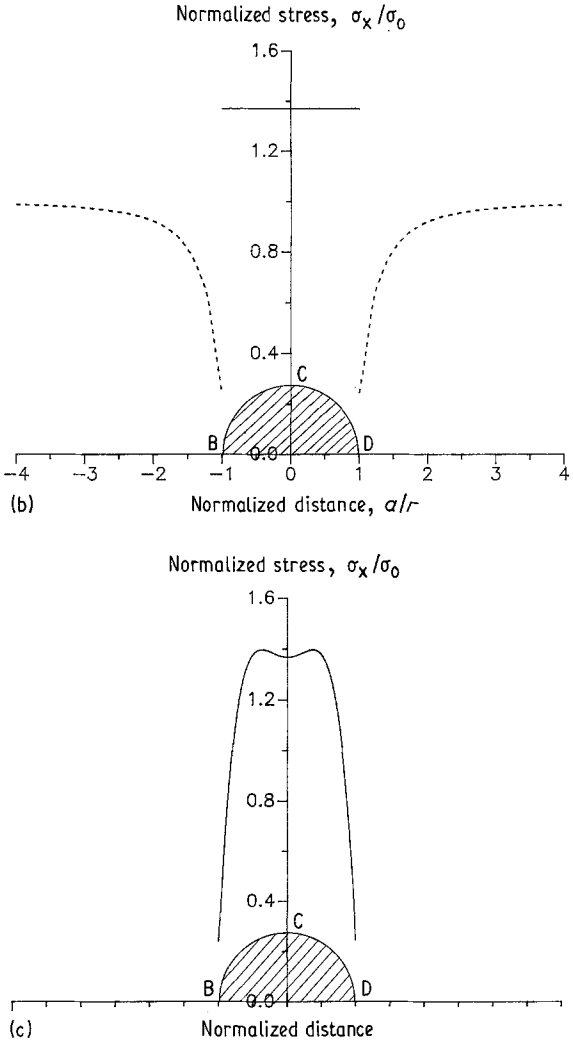

Figure 5 Normalized stress (σ_x/σ_0) distribution in the region of circular SiC_p and 6061 Al alloy (a) Schematic illustration of the loading configuration and the trajectory along which stress distributions are drawn. (b) Along the line ABODE, (——) inclusion, (– – –) matrix. (c) Along the interface BCD. The shaded semi-circle in (b) and (c) indicates the location of the particulate.

acting on the matrix near the pole of the inclusion is calculated to be about 1.5 times that of the applied tensile stress. This stress reaches a maximum value in the matrix at a point slightly away from the pole along the direction of the applied stress, and finally decreases to the level of applied tensile stress at regions away from the pole. Such a stress distribution at the pole region of the inclusion, along the direction of the tensile stress, appears to be responsible for some of the matrix material to be adherent to the particulate reinforcement, as has been observed occasionally at the debonded interfaces (Fig. 3b). This stress distribution is illustrated in Fig. 7.

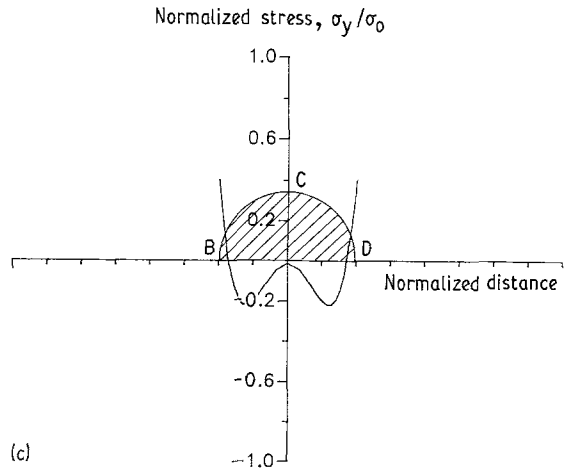

Figure 6 Normalized stress (σ_y/σ_0) distribution in the region of circular SiC_p and 6061 Al alloy. (a) Schematic illustration of the loading configuration and the trajectory along which stress distributions are drawn. (b) Along the line ABODE, (——) inclusion, (– – –) matrix. (c) Along the interface BCD, (——) interface. The shaded semi-circle in (b) and (c) indicates the location of the particulate.

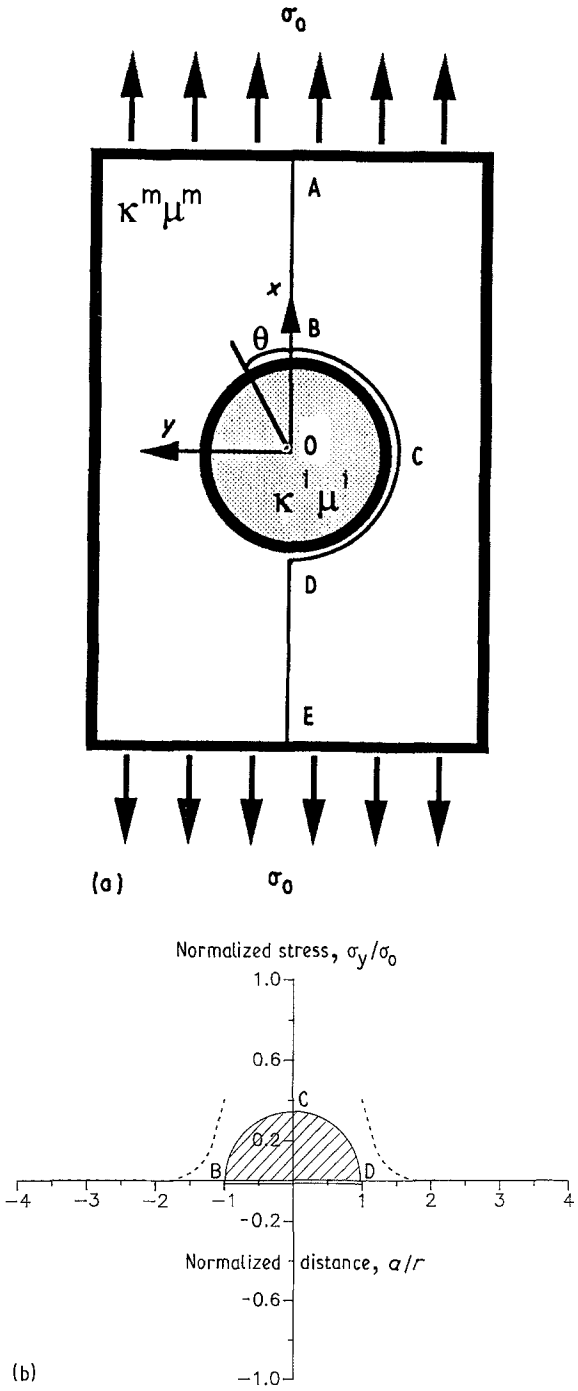

TABLE III Selected material properties for SiC and Al_2O_3 [28]

Material	E(GPa)	μ(GPa)	ν	α (10^{-6} °C^{-1})
6061 Al	68.0	29.3	0.33	28.0
SiC	423.0	178.0	0.19	3.0
Al_2O_3	396.9	160.2	0.24	6.5

5.2. Interfacial debonding and particulate cracking

The axial stress developed in the matrix along the matrix/inclusion interface, σ^m_{xx}, increases significantly at the region of the pole of the inclusion, and decreases very rapidly as the angle, θ, measured from the pole rotates and approaches 90°, while the stress inside the inclusion remains constant, as shown in Fig. 5. Such a stress concentration at the inclusion and the matrix/inclusion interface can cause particulate cracking and interfacial debonding, respectively. Using Equations 4 and 10, the maximum stress in the matrix near the pole of SiC_p is calculated to be about 1.5 times the applied tension, assuming plane stress conditions. With a tensile stress of 300–400 MPa, the typical strength of such composites, the stress at the pole of SiC_p reaches about 450–600 MPa. Although such a stress is not large enough compared to the interfacial bonding strength of SiC and aluminium reported by Flom and Arsenault [29], interfacial debonding may occur due to the imperfect interface present in the composites. The formation of an intermetallic compound [30] or amorphous phase [26] can cause degradation of the interface. Sharp corners [21] will result in higher stress concentration. Incipient debonding at the interface as a consequence of the manufacture results in severe stress concentration, as shown in Fig. 8. Once interface is debonded at the pole of SiC_p, the crack so formed will propagate along the SiC_p/Al interface to some extent and then deviate into

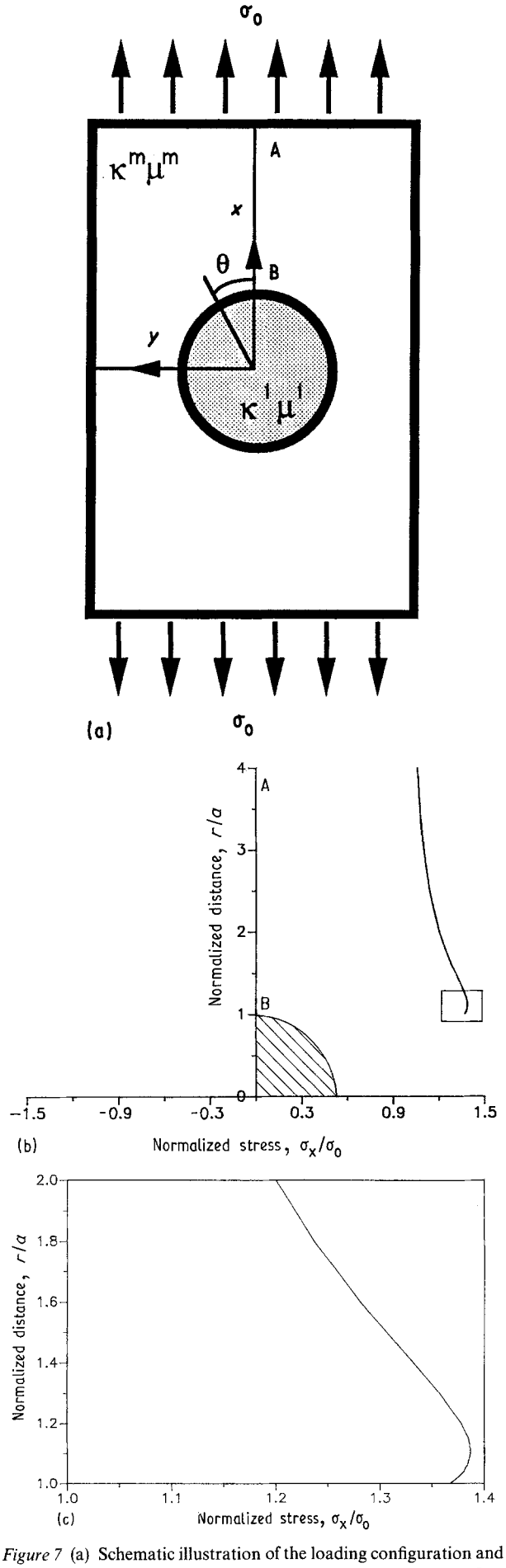

Figure 7 (a) Schematic illustration of the loading configuration and the trajectory along which stress distributions are drawn. (b) Normalized stress (σ_x/σ_0) distribution from the pole of SiC_p along the line AB (tensile direction). (c) Detailed stress distribution pattern within the enclosed rectangle. The shaded quarter-circle in (b) indicates the location of the particulate.

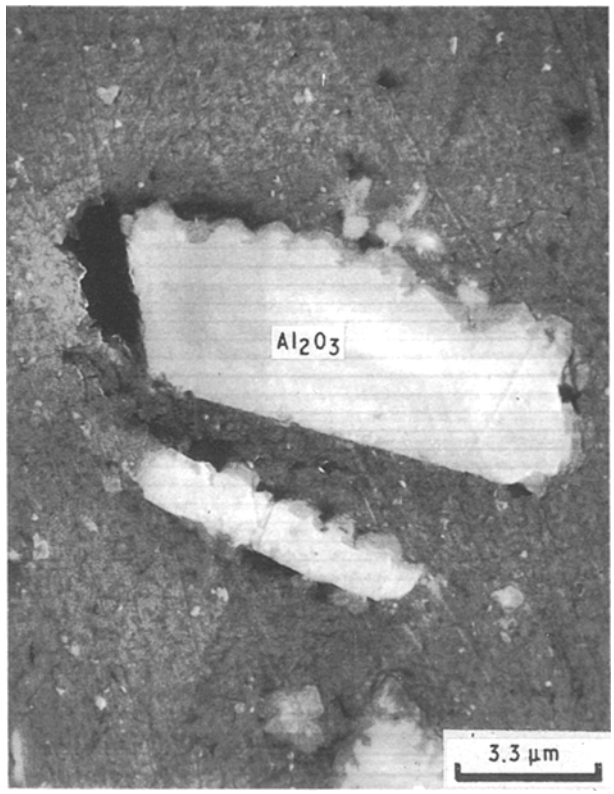

Figure 8 Scanning electron micrograph showing the incipient debonding and compound layer observed in $(Al_2O_3)_p/Al$ composite. The micrograph was taken from the surface perpendicular to the extrusion direction.

the matrix. This is due to the fact that the axial stress, σ_{xx}, at the interface decreases and that in the matrix increases abruptly as can be seen in Fig. 5.

Tensile loading also gives rise to stress concentration within SiC_p, causing particulate cracking. From Equations 4 and 10, the stress exerted on SiC_p is calculated to be about 1.5 times that of the applied tensile stress. Although, this calculated stress is smaller than the fracture strength of SiC, its failure can occur even under a small stress value, because most ceramic particles have flaws, grain boundaries, and sharp points where higher stress is concentrated. From Fig. 3, which illustrated typical particulate cracking under tension, one can notice that particulate cracking precedes matrix failure, although severe plastic deformation could be observed in the matrix near the region of cracked SiC_p. Once SiC_p has cracked, the constraint on the plastic deformation of the matrix will disappear. Then matrix near SiC_p can easily undergo plastic deformation. Such a situation can be considered to be similar to the matrix alloy with a crack in it, providing a higher stress concentration at the crack tip. Under such conditions, the matrix fails easily, and the ductility of the composite will decrease significantly.

5.3. Effect of thermal residual stress on the failure mode

In this specific case, the pressure acting on the matrix/inclusion interface ($-P$ in Equation 7) is computed to be about -800 MPa for the temperature

drop from the composite fabrication temperature to room temperature ($\Delta T \approx 600\,^{\circ}C$). However, upon cooling from the fabrication temperature, most of this inelastic stress will be relieved by the plastic deformation of the matrix near SiC_p (i.e. generation of dislocation around SiC_p) and only a small portion of about -30 MPa, as estimated by Arsenault and Taya [31], will remain in the form of residual stress at the interface. These inelastic stresses acting on SiC_p and the matrix will not change the state of stress significantly, because values are small compared to those of the applied stress. Consequently, there should be no substantial changes in the mode of particulate cracking and interfacial debonding as a result of the thermal residual stress.

5.4. Proposed failure modes

Based on the present study, the failure mechanism of the particulate-reinforced aluminium alloy composites can be summarized as follows. When a composite system is subjected to uniaxial tension, the maximum tensile stress is generated at the reinforcement and matrix near the pole of the reinforcement, in the same direction to the applied tension. Such a stress concentration may cause particulate cracking or interfacial debonding. As loading continues, the particulate cracks and debonded interfaces easily open up due to the plastic deformation of the matrix near the reinforcement. New cracks will develop in the matrix at the tip of the opened-up crack and propagate into the matrix until they are joined with nearby cracks, resulting in a large void. Schematic representations of various steps for this failure mode are illustrated in Fig. 9.

The micrographs of the side surfaces of tensile specimens adjacent to the fractured region are given in Figs 1, 2 and 3. Extensive particulate crackings and debonded interfaces can be observed in these micrographs. Joining of nearby cracks into a large crack can also be observed in Fig. 1. The void formation, as a result of such coalescences, can be seen in Fig. 2. Based on these observations, particulate cracking, in addition to interface debonding, can be proposed as a major contributor to the failure of the particulate-reinforced aluminium alloy composites.

6. Conclusions

Stress concentration in the matrix near the pole of the particulate, and stress concentration within the particulate, appear to result in interfacial debonding and particulate cracking, respectively. Increase in applied stress causes such microcracks to open. New cracks develop in the matrix at the tip of the opened-up crack, propagate into the matrix and join with nearby cracks, and form a large void. Based on the microscopic examinations and analytical study, interfacial debonding and particulate cracking together were considered to be responsible for the substantial decrease in the ductility of the particulate-reinforced aluminium alloy composites.

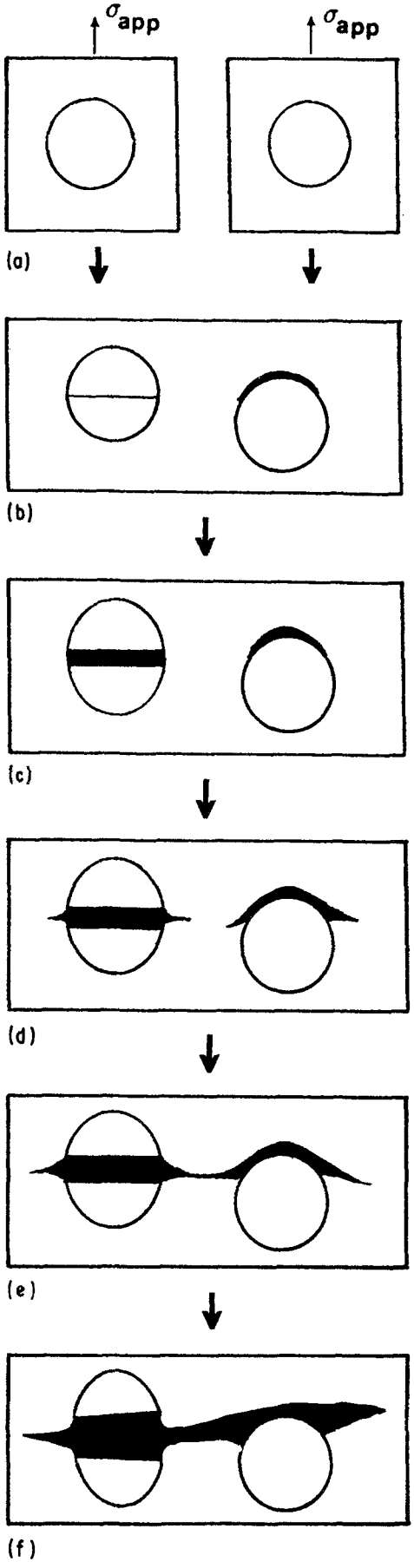

Figure 9 Schematic drawings of the failure mechanism of the particulate-reinforced aluminium alloy composites. (a) Loading configuration. (b) Formation of particulate cracking and interfacial debonding. (c) Opening-up of cracked plane and debonded interface due to plastic flow of the aluminium matrix. (d) Crack propagation into the aluminium matrix due to stress concentration build-up at the crack tip. (e) Joining of cracks. (f) Void formation.

Because particulate cracking and interfacial debonding were observed to always precede the matrix failure, such phenomena appear to be more responsible for the failure than a mechanism based on the matrix failure

References

1. N. TSANGARAKIS, B. O. ANDREWS and C. CAVALLARO, *J. Compos. Mater.* **21** (1987) 481.
2. T. G. NIEH and D. J. CHELLMAN, *Scripta Metall.* **18** (1984) 925.
3. R. J. ARSENAULT and S. B. WU, *ibid.* **22** (1988) 767.
4. R. J. ARSENAULT, *Mater. Sci. Engng* **64** (1981) 171.
5. Y. FLOM and R. J. ARSENAULT, *J. Metals* **38** (1986) 31.
6. V. C. NARDONE, *Scripta Metall.* **21** (1987) 1313.
7. R. H. JONES, C. A. LAVENDER and M. T. SMITH, *ibid.* **21** (1987) 1565.
8. W. A. LONGSDON and P. K. LIAW, *Engng Fract. Mech.* **24** (1986) 737.
9. T. CHRISTMAN and S. SURESH, *Mater. Sci. Engng* **102** (1988) 211.
10. J. K. SHANG, W. YU and R. O. RITCHIE, *ibid.* **102** (1988) 818.
11. F. M. HOSKING, F. F. PORTILLO, R. WUNDERLIN and R. MEHRABIAN, *J. Mater. Sci.* **17** (1982) 477.
12. F. A. GIROT, J. M. QUENISSET and R. NASLAIN, *Compos. Sci. Technol.* **30** (1987) 155.
13. V. C. NARDONE and J. R. STRIFE, *Metall. Trans.* **18A** (1987) 109.
14. K. S. RAVICHANDRAN, *J. Metals* **39** (1987) 28.
15. J. J. STEPHENS, J. P. LUCAS and F. M. HOSKING, *Scripta Metall.* **22** (1988) 1307.
16. D. L. McDANELS, *Met. Trans.* **16A** (1985) 1105.
17. R. J. ARSENAULT and S. B. WU, *Mater. Sci. Engng* **96** (1987) 77.
18. A. K. VASUDEVAN, O. RICHMOND, F. ZOK and J. D. EMBURG, *ibid.* **A107** (1989) 63.
19. H. OHTSU, "Design and manufacturing of advanced composites" (ASM, Detroit, 1989) p. 187.
20. D. J. LLOYD, H. LAGACE, A. McLEOD and P. L. MORRIS, *Mater. Sci. Engng* **A107** (1989) 73.
21. S. R. NUTT and J. M. DUVA, *Scripta Metall.* **20** (1986) 1055.
22. S. R. NUTT and A. NEEDLEMAN, *ibid.* **21** (1987) 705.
23. J. J. LOWANDOWSKI, C. LIU and W. H. HUNT, *Mater. Sci. Engng* **107A** (1989) 241.
24. C. P. YOU, A. W. THOMPSON and I. M. BERNSTEIN, *Scripta Metall.* **21** (1987) 181.
25. T. CHRISTMAN, A. NEEDLEMAN, S. NUTT and S. SURESH, *Mater. Sci. Engng* **107A** (1989) 49.
26. G. M. JANOWSKI and B. J. PLETAKA, *ibid.* **A129** (1990) 65.
27. N. I. MUSKHELISHVILI, "Some basic problems of the mathematical theory of elasticity" (Noordhoff, Groningen, Holland, 1953) pp. 215–16.
28. Y. S. TOULOUKIAN (ed.) "Thermophysical properties of high temperature solid materials, Vol. 6, part I (Thermophysical properties research center, Purdue University, 1967).
29. Y. FLOM and R. J. ARSENAULT, *Mater. Sci. Engng* **77** (1986) 191.
30. T. ISEKI, T. KAMEDA and T. MARUYAMA, *J. Mater. Sci.* **19** (1984) 1692.
31. R. J. ARSENAULT and M. TAYA, *Acta Metall.* **35** (1987) 651.

Received 17 June
and accepted 16 December 1991